Journal of Computational Acoustics

DIFFRACTION OF AN ACOUSTIC WAVE BY A PLATE IN A UNIFORM FLOW: A NUMERICAL APPROACH

S. JOB[†⋆*], E. LUNÉVILLE[†] and J.-F. MERCIER[†]

[(†)] *ENSTA, POems,UMR 2706-CNRS, 32 bd Victor, 75739 PARIS Cedex 15, France.*

[(⋆)] *LAUM, UMR 6613-CNRS, Université du Maine, Avenue O. Messiaen, 72085 Le Mans Cedex 9, France. sjob@usach.cl, lunevill@ensta.fr, jmercier@ensta.fr*

http://www.ensta.fr/uer/uma/labo/index.html

Received (Day Month Year)
Revised (Day Month Year)

We study the diffraction in time harmonic regime of an acoustic wave by a rigid plate in the presence of a uniform flow in a duct. Contrary to prior analytical studies, using Wiener-Hopf techniques and thus restricted to semi-infinite plates, we use a finite elements method which allows us to deal with plates of finite length. To take into account irrotational perturbations induced by the trailing edge of the plate, a potential formulation requires the introduction of a vortex sheet behind the plate. The key point of the method is to get access at the singular coefficient of the velocity potential near the trailing edge, in order to cancel it using the so-called Kutta-Joukowski condition. This approach leads to an efficient finite elements method, and numerical computations are presented: we show the amplitude of the vortex sheet versus the Mach number and the plate length and the dissipated acoustic power versus the Mach number and the frequency. This method is extended to the case of two aligned plates to analyze the influence of the choice of the boundary condition on the downstream plate which interacts with a vortex sheet.

Keywords: acoustic-flow interaction; diffraction by a plate; finite elements method.

1. Introduction

We are interested in the diffraction of an acoustic wave by plates of finite length in presence of a uniform flow confined in a duct. Such studies can help to improve the design of aeroacoustic devices, for example, absorbing linings used for the reduction of noise radiated from aeroengines or ventilation fans.

As a model of perforated screens, the case of aligned plates is of practical importance. These screens are used to attenuate aerodynamic sound in heat-exchanger cavities or other industrial devices conveying mean flow. Their effectiveness is due to the vorticity production by the sound within the perforations, the kinetic energy of the vortex field being extracted from the sound. This mechanism has been investigated both theoretically [1] and experimentally [2], but these studies were restricted to the case of an infinite thin plate having a single transverse slot. The influence of vorticity ejection into the flow has been used to

*Current affiliation: CIMAT, Universidad de Chile, AV. Blanco Encalada 2008, Santiago de Chile.

examine mean-flow/acoustic energy exchanges and it has been found both experimentally and theoretically that the dissipation is greatly enhanced by flow.

This paper follows the paper [3] which presented a 2D potential model in the time harmonic regime based on the linear Euler's equations for the case of one plate. In that paper [3] a rigourous mathematical analysis was given and a first numerical method was suggested. Our aim is to extend this numerical method to low Mach numbers and to deal with more interesting cases such as aligned plates, which involve original modelization questions.

Acoustic diffraction in the presence of a flow is more complicated than in the case without a flow, since a coupling between the acoustic and hydrodynamic perturbations occurs which requires an understanding of the physical mechanisms involved. Without any flow, the velocity perturbations are curl free everywhere in the fluid. On the other hand, in the case of a plate in a flow, the coupling between the incident acoustic wave and the flow induces rotational velocity perturbations behind the plate. The usual modelization consists of introducing a vortex sheet behind the plate [4,5,6,7] and then imposing a Kutta-Joukowski condition at the trailing edge to determine the intensity of this vortex sheet as in thin aerofoil theory [8]. This model, inviscid since Euler's equations are considered, was proven to be consistent with more complete viscous models, examples of which include an analytical model consisting of determining the asymptotic boundary layer structure (triple deck theory) near a plate trailing edge [9,10] and a "numerical" model based on the time dependant Euler's equations where the numerical dissipation induces a wake [11]. Models other than a complete model may also be considered: for example, the compressible Navier-Stokes equations contain all the interesting phenomena but a numerical scheme based on this idea is very complicated to develop and is generally restricted to objects that are small compared to the wavelength [12,13].

As already noted in a previous paper [3] the acoustic diffraction by a plate raises some modelization and numerical difficulties. Briefly, the Kutta-Joukowski condition at the trailing edge requires us to deal with a potential formulation which is split betweens an "acoustic" part and a "vortex sheet" part. In this linear decomposition, the amplitude of the vortex sheet part, denoted F, appears as a new unknown of the problem and is determined by the Kutta-Joukowski condition. The amplitude F is in fact the ratio of the singularity coefficients of the acoustic field and the vortex sheet field. In addition, as the vortex sheet extends to infinity, there is no obvious radiation condition and the decomposition we use allows us to take into account the standard acoustic radiation conditions. Lastly, a spectral approximation of the fields is used close to the edges in order to evaluate F at the trailing edge, and also to get more accurate approximations at the leading edge than provided by the finite elements method. Of course, the poor convergence of finite elements methods for domains with edges is well known and other techniques are possible (local mesh refinement [14], for example).

Our major interest is the diffraction by a finite plate and, in particular, the evolution of the vortex sheet when the flow velocity decreases. Indeed there is no vortex sheet in the case without flow, but the vortex sheet exhibits a non-trivial behavior in presence of

a flow whose velocity tends to zero. It becomes very oscillating along the flow direction and the field radiated by the sheet has an exponential boundary layer behavior in the transverse direction. The numerical method used in the previous paper [3] was unable to deal with low Mach numbers, because of the presence of numerical instabilities due to the exponential growth of the vortex sheet extension function used in the finite elements method. We propose here to use a new extension method for which the exponential growth is under control. To understand the transition from the case of a flow with negligible velocity to the case without flow, the evolution of the wake amplitude is numerically determined. Note that the behavior of the vortex sheet as the Mach number tends to zero for a semi-infinite plate may be obtained by Wiener-Hopf techniques [4,5,6,7]. However, for a finite plate, a Wiener-Hopf method no longer leads to semi-analytical results [15], but to an alternative numerical method which appears too intricate to extend to more complicated situations (aligned plates for exemple).

Finally, the case of two aligned plates will also be considered. This configuration introduces two new interactions: one between the vortex sheets produced by the two plates, and another between the vortex sheet produced by the upstream plate with the leading edge of the downstream plate. This second interaction is not obvious and several boundary conditions on the downstream plate have been proposed [16,17]. We will study the influence of these boundary conditions on the diffracted field.

The paper is organized as follows. In section 2 we present the equations of the diffraction problem and the "vortex sheet elimination" procedure. Section 3 concerns the presentation of the numerical method and in particular the coupling between finite elements and modal expansions. Finally in section 4 we report the results: the behavior of the vortex sheet for low Mach numbers in the one plate case, and the influence of an extra plate on the diffracted acoustic field.

2. Model

2.1. *Geometry and equations*

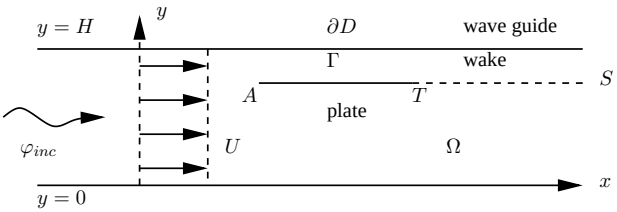

Fig. 1. Geometry of the problem.

We consider a two-dimensional problem, where x and y are respectively the horizontal and vertical axis (see Fig. 1). The duct is defined as the domain $D = \mathbb{R} \times]0, H[$, where H is

the height of the duct. The plate of length L is defined as $\Gamma = \{(x, y); y = \eta \text{ and } 0 < x < L\}$, where $0 < \eta < H$. The velocity of the flow is noted U and we consider small acoustic perturbations of the uniform flow: the velocity $\mathbf{v}$ of the acoustic perturbations and the acoustic pressure field p satisfy the linearized isentropic Euler equations in $\Omega = D\backslash\Gamma$:

$$\begin{cases} \rho \dfrac{D\mathbf{v}}{Dt} + \nabla p = 0, \\ \dfrac{1}{c^2}\dfrac{Dp}{Dt} + \rho \operatorname{div} \mathbf{v} = 0. \end{cases} \tag{1}$$

ρ is the fluid density and c is the sound velocity, both defined in the fluid at rest. We consider a time harmonic regime $e^{-i\omega t}$ where ω is the frequency of the incident wave. Then the convective derivative takes the form $D/Dt = -i\omega + U\partial/\partial x$. The boundary conditions are the slip condition on the plate and on the rigid walls $\mathbf{v} \cdot \mathbf{n} = 0$ where $\mathbf{n}$ is the unit vector outside Ω.

2.2. *Vortex sheet*

Let us determine where the velocity perturbations are curl free. From Eq. 1 is deduced that the vorticity perturbation curl $\mathbf{v}$ is only convected by the mean flow $(D/Dt)\text{curl}\,\mathbf{v} = 0$. If the fluid is at rest ($U = 0$), the velocity perturbations are curl free everywhere. If $U \neq 0$, we get that $(M\partial/\partial x - ik)$ curl $\mathbf{v} = 0$ where $M = U/c$ is the Mach number (taken in the range $0 < M < 1$) and $k = \omega/c$ is the acoustic wavenumber. Thus, if the incident wave is supposed curl free, curl $\mathbf{v} = 0$ everywhere except behind the plate, where a vortex sheet $S = \{y = \eta, x > L\}$ develops (the general solution in Ω is curl $\mathbf{v} = f(y)e^{ikx/M}$ where f is given by the value of the vorticity at a point downstream the plate). The boundary conditions on the vortex sheet are $[u_y]_S = 0 = [p]_S$ where $[.]_S$ denotes the jump through the vortex sheet ($[\varphi]_S = \varphi(x, \eta + 0) - \varphi(x, \eta - 0)$) and where $\mathbf{u}$ is the fluid displacement perturbation, defined by $D\mathbf{u}/Dt = \mathbf{v}$ (see [4,5,6,7]).

2.3. *Diffraction problem*

Eliminating the velocity in Eq. 1 leads to the convective wave equation for the velocity potential:

$$H_M(\varphi) = (1 - M^2)\frac{\partial^2\varphi}{\partial x^2} + \frac{\partial^2\varphi}{\partial y^2} + 2ikM\frac{\partial\varphi}{\partial x} + k^2\varphi = 0 \text{ in } \Omega\backslash S.$$

We are interested in the diffracted field when the plate is submitted to an incident wave φ_{inc}. Then the total field is sought in the form $\varphi = \varphi_{inc} + \varphi_d$ and the diffracted velocity potential φ_d must satisfy:

$$\begin{cases} H_M(\varphi_d) = 0 & \text{in } \Omega\backslash S, \\ \partial\varphi_d/\partial y = 0 & \text{on } \partial D, \\ \partial\varphi_d/\partial y = -\partial\varphi_{inc}/\partial y & \text{on } \Gamma, \end{cases} \tag{3}$$

and radiation conditions too. On the vortex sheet, the continuity of the normal component of the displacement leads to $[\partial\varphi_d/\partial y]_S = 0$. Using Eq. 1, the link between the pressure and the velocity potential is obtained and the continuity of the pressure leads to $(M\partial/\partial x - ik)\,[\varphi_d]_S = 0$ which implies $[\varphi_d]_S = Fe^{ikx/M}$ where F is an unknown constant. It will be determined by applying the Kutta-Joukowski condition at the trailing edge $T\,(L,\eta)$.

2.4. *Transformation uniform flow-medium at rest*

To simplify the problem, we use a change of variables and unknown which allows us to transform the equations of acoustics in a uniform flow into the equations of acoustics in a medium at rest (Prandtl-Glauert transformation). If we set $\hat{x} = x/\sqrt{1-M^2}$, $\hat{y} = y$, $\alpha = k/\sqrt{1-M^2}$ and $\hat{\varphi}(\hat{x},\hat{y}) = \varphi(x,y)e^{i\alpha M\hat{x}}$, Eq. 3 becomes

$$\begin{cases} (\Delta+\alpha^2)\hat{\varphi}_d = 0 & \text{in } \hat{\Omega}/\hat{S}, \\ \partial\hat{\varphi}_d/\partial y = 0 & \text{on } \partial\hat{D} \quad \text{and} \quad \partial\hat{\varphi}_d/\partial y = -\partial\hat{\varphi}_{inc}/\partial y \ \text{ on } \hat{\Gamma}, \\ [\hat{\varphi}_d]_{\hat{S}} = Fe^{i\alpha\hat{x}/M} & \text{and } \ [\partial\hat{\varphi}_d/\partial y]_{\hat{S}} = 0, \end{cases} \tag{4}$$

where the new domains are dilated comparing to initial domains. The plate length becomes $\hat{L} = L/\sqrt{1-M^2}$. The classical Helmholtz equation is recovered and we are led to solve the diffraction problem in a medium at rest but with a larger acoustic frequency α instead of k and in a new geometry (longer plate). This transformation presents a numerical advantage: it allows us to access in a simpler way to the singularity coefficients of the diffracted field thanks to a representation in series of the solution near the end edges of the plate (section 3). Nevertheless this transformation leads to a numerical problem: if we note λ the wake wavelength in the medium with flow, it becomes $\hat{\lambda} = \lambda\sqrt{1-M^2}$ in the medium at rest. Thus when $M \to 1$, $\hat{\lambda} \to 0$ which necessitates to reduce the step of the mesh.

Since we will now concentrate on the resolution of Eq. 4, we will drop the "hats" $\hat{}$ in the following of the paper.

2.5. *Modes of the duct*

The radiation conditions at infinity (the diffracted field must go away from the plate) are expressed thanks to the modes of the duct, which we will calculate now. The modes of the duct (without the plate) are the solutions of $(\Delta+\alpha^2)\varphi = 0$ in D with $\partial\varphi/\partial y = 0$ on ∂D and with separated variables. They are well known [18] and read $\varphi_n^{\pm}(x,y) = e^{\pm i\beta_n x}\cos(n\pi y/H)$, where the wave numbers are given by $\beta_n = \sqrt{\alpha^2-(n\pi/H)^2}$ if $0 \le n \le \alpha H/\pi$ (then $\varphi_n^{\pm}$ is a propagative mode) and $\beta_n = i\sqrt{(n\pi/H)^2-\alpha^2}$ if $n \ge \alpha H/\pi$ (then $\varphi_n^{\pm}$ is an evanescent mode). The group velocity is positive for φ_n^{+} modes and negative for φ_n^{-} ones.

Finally we should impose some radiation condition to ensure the well-posedness of problem 4. Because of the presence of a vortex sheet, it is complicated to find some well-suited radiation condition. To overcome this difficulty, in the next paragraph we will "eliminate" the vortex sheet by spliting the problem.

2.6. *Spliting of the problem*

We introduce the unitary vortex sheet function φ_S satisfying:

$$\begin{cases} (\Delta + \alpha^2)\varphi_S = 0 & \text{in } \Omega/S, \\ \partial\varphi_S/\partial y = 0 & \text{on } \partial D \cup \Gamma, \\ [\varphi_S]_S = e^{i\alpha x/M} & \text{and} \quad [\partial\varphi_S/\partial y]_S = 0. \end{cases} \tag{5}$$

φ_S is the acoustic field diffracted by a vortex sheet of amplitude $F = 1$. Then the diffracted field may be sought in the form $\varphi_d = \varphi_a + F\varphi_S$, where φ_a satisfies a problem without vortex sheet. Note that in the case of an inviscid incompressible flow around an airfoil, a vortex sheet is also present and the problem of finding the velocity potential in presence of a vortex sheet is also splitted in two problems without vortex sheet [8]. Since φ_a is a purely irrotational solution (i.e. corresponds to $F = 0$) of the diffraction problem, it is called the acoustic part of the diffracted field, whereas φ_S is the vortical field.

The total acoustic field $\varphi = \varphi_{inc} + \varphi_a$ is solution of:

$$\begin{cases} (\Delta + \alpha^2)\varphi = 0 & \text{in } \Omega, \\ \partial\varphi/\partial y = 0 & \text{on } \partial D \cup \Gamma, \end{cases} \tag{6}$$

with radiation condition at infinity for $\varphi - \varphi_{inc}$. Except for the particular case $M = 0$, it is not the right physical solution since it does not satisfy the Kutta-Joukovski condition. We introduce the "vortex sheet" extension function $\tilde{\varphi}_S$ defined as $\tilde{\varphi}_S = \Theta(x)\zeta(y)e^{i\alpha x/M}$, where

$$\zeta(y) = \begin{cases} \zeta^-(y) = A\cosh(ky/M) & \text{if } y < \eta, \\ \zeta^+(y) = B\cosh[k(H-y)/M] & \text{if } y > \eta. \end{cases}$$

$\Theta(x)$ is a truncature function such that $\Theta(x) = 0$ if $x < d$ and $\Theta(x) = 1$ if $x > d$, where $0 < d < L$, $A = -\sinh[k(H-\eta)/M]/\sinh[kH/M]$ and $B = \sinh(k\eta/M)/\sinh(kH/M)$. A et B are determined such that $\tilde{\varphi}_S$ is associated to a vortex sheet of amplitude $F = 1$: $[\tilde{\varphi}_S]_S = e^{i\alpha x/M}$ and $[\partial\tilde{\varphi}_S/\partial y]_S = 0$. $\zeta(y)e^{i\alpha x/M}$ is represented for $\eta = H/2$, $M = 0.4$ and $M = 0.1$ on Fig. 2. The singular behavior of the vortex sheet function appears clearly for $M = 0.1$: $\tilde{\varphi}_S$ becomes very thin vertically and very oscillating horizontally. Note that since the unitary vortex sheet function remains bounded as $M \to 0$, it "disappears" when M vanishes (tends to zero nearly everywhere). But $F(M)$ could tend to infinity when $M \to 0$, and so the transition from a model with flow to a model without flow is not obvious.

$\tilde{\varphi}_S$ is solution of the vortex sheet equations Eq. 5 but does not satisfy the right boundary condition on the plate $\partial\tilde{\varphi}_S/\partial y \neq 0$ on Γ. Therefore to obtain φ_S, we need to introduce the correction function φ_c defined as $\varphi_S = \tilde{\varphi}_S + \varphi_c$. Since we have considered a Heaviside function Θ in the definition of the vortex sheet extension function $\tilde{\varphi}_S$, we introduce the two domains $\gamma_+ = \{(d, y); \eta < y < H\}$ and $\gamma_- = \{(d, y); 0 < y < \eta\}$ on which we have to set the adapted transmission conditions. Like the acoustic field φ_a, the correction function is solution of a diffraction problem without vortex sheet, similar to Eq. 6:

$$\begin{cases} (\Delta + \alpha^2)\varphi_c = 0 & \text{in } \Omega, \\ \partial\varphi_c/\partial y = 0 & \text{on } \partial D \text{ and } \partial\varphi_c/\partial y = -\partial\tilde{\varphi}_S/\partial y \text{ on } \Gamma, \\ [\varphi_c]_{\gamma_\pm} = -\tilde{\varphi}_S|_{\gamma_\pm}, & \text{and } [\partial\varphi_c/\partial x]_{\gamma_\pm} = -i\,\alpha\tilde{\varphi}_S/M|_{\gamma_\pm}. \end{cases} \tag{7}$$

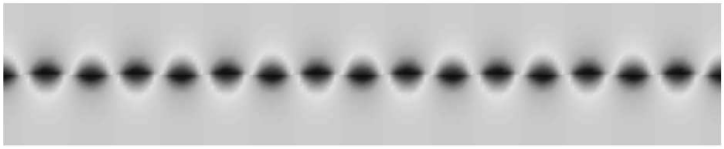

(a) $M = 0.4$

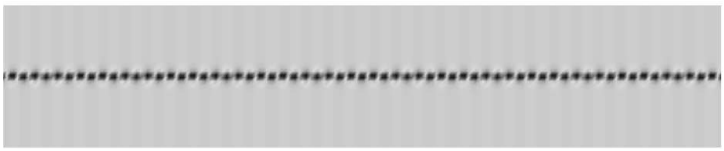

(b) $M = 0.1$

Fig. 2. $\zeta(y)e^{i\alpha x/M}$ for two values of the Mach number

From Eq. 7 it is obvious that numerical problems appear when $M \to 0$. If we note λ_S the vortex sheet wavelength satisfying $2\pi/\lambda_S = \alpha/M$, we get that $\lambda_S \to 0$ when $M \to 0$. Thus the source term $\partial\tilde{\varphi}_S/\partial y$ on Γ becomes very oscillating for weak fluid velocity, which necessitates to refine the mesh near Γ.

The following is devoted to the determination of φ and φ_c, respectively solution of Eq. 6 and Eq. 7. If these problems are solved thanks to finite elements, the approximation is inaccurate: indeed if h denotes the discretisation step, we get an error of order h^α with $0 < \alpha < 1/2$ instead of $\alpha = 1$ as usually encountered. This difference is due to the singularities of φ or φ_c near the edges of the plate. To improve the accuracy of the numerical method, the diffracted field near the edges of the plate is calculated using a spectral approximation which has better convergence properties [19] (error even exponentially decreasing when the number of terms in the serie increases). Moreover this spectral decomposition will give a simple access to the amplitude F of the vortex sheet.

3. Numerical scheme

A bounded domain Ω_R surrounding the plate is introduced: $\Omega_R = \{(x, y) \in \Omega; |x| < R\}$, where $R > L$ (see Fig. 3). This domain is delimited by the two boundaries $\Sigma_\pm = \{(x, y); x =$

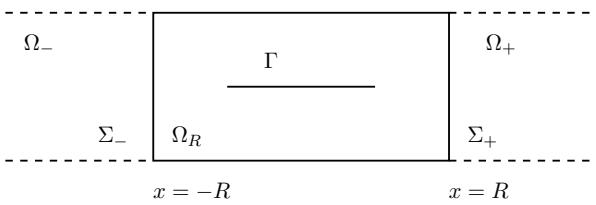

Fig. 3. Reduction of the diffraction problem to a bounded domain Ω_R.

$\pm R$ and $0 < y < H\}$. The diffracted fields will be determined in the bounded domain. Outside Ω_R we prove in the following that the diffracted field can be found thanks to modal decompositions.

3.1. *Modal representations in the exterior domains*

We introduce the exterior domains $\Omega_\pm = \{(x,y) \in \Omega; \pm x > R\}$. If we note $\varphi_\pm$ the solution of Eq. 6 or of Eq. 7 in $\Omega_\pm$, the modal representations of these solutions are given by:

$$\varphi_\pm = \sum_{n=0}^{\infty} (\varphi_\pm, \theta_n)_{\Sigma_\pm} \, e^{\pm i\beta_n(x \mp R)} \theta_n(y) \text{ in } \Omega_\pm,$$

where the functions $\theta_n(y)$ are defined as $\theta_n(y) = \sqrt{2/H}\cos(n\pi y/H)$ if $n \geq 1$, $\theta_0(y) = 1/\sqrt{H}$, and the scalar product introduced on the boundaries $\Sigma_\pm$ is $(\varphi,\psi)_{\Sigma_\pm} = \int_{\Sigma_\pm} \varphi\bar{\psi}dy$. Note that the functions $\varphi_\pm$ satisfy the outgoing wave condition. As a consequence if we note ϕ the solution φ of Eq. 6 or the solution φ_c of Eq. 7 in Ω_R, using the continuity of ϕ and of $\partial\phi/\partial x$ through $\Sigma_\pm$, it satisfies the boundary condition $\partial\phi/\partial n = -T_{\Sigma_\pm}(\phi)$ on $\Sigma_\pm$, where the Dirichlet-to-Neumann operators $T_{\Sigma_\pm}$ are defined as follows:

$$T_{\Sigma_\pm}\phi = -i \sum_{n=0}^{\infty} \beta_n(\phi, \theta_n)_{\Sigma_\pm} \, \theta_n(y),$$

$\mathbf{n}$ being the outgoing normal of Ω_R.

Similar spectral representations and boundary conditions can be deduced when looking for the diffracted fields near the end edges of the plate, and are presented in the next paragraph.

3.2. *Spectral representations in the interior domains*

Two disks $D_\pm$ of radius ρ are built around the edges of the plate in $x = 0$ and $x = L$ (Fig. 4). The plate Γ is splitted in three parts: the end parts $\Gamma_\pm = \Gamma \cap D_\pm$ and the middle of

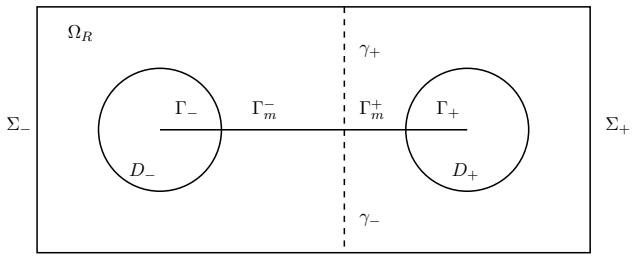

Fig. 4. Bounded domains built near the plate end edges.

the plate $\Gamma_m = \Gamma \backslash (\Gamma_+ \cup \Gamma_-)$. We note $\varphi_{D_\pm}$ the solution of Eq. 6 or of Eq. 7 in $D_\pm$. Because

of the presence of the vertical boundaries $\gamma_\pm$, the middle part of the plate is also splitted in two pieces $\Gamma_m^+ = \{(x,\eta) \in \Gamma_m; x > d\}$ and $\Gamma_m^- = \{(x,\eta) \in \Gamma_m; x < d\}$.

3.2.1. *Left disk D_-*

If we define the polar coordinates with a radius $r = \sqrt{x^2 + (y-\eta)^2}$ and an angle $\theta \in [0, 2\pi[$, φ_{D_-} is proven to read:

$$\varphi_{D_-}(r,\theta) = \sum_{n=0}^{\infty} \frac{J_{\frac{n}{2}}(\alpha r)}{J_{\frac{n}{2}}(\alpha\rho)} (\varphi_{D_-}, b_n)_{\partial D_-} b_n(\theta) \text{ in } D_-\backslash\Gamma_-, \tag{8}$$

where J_n is the n^{th} Bessel function, ∂D_- is the boundary of the disk D_- and the functions $b_n(\theta)$ are defined as $b_n(\theta) = \cos(n\theta/2)/\sqrt{\pi\rho}$ if $n \geq 1$, $b_0(\theta) = 1/\sqrt{2\pi\rho}$. In order not to divide by zero, the radius is chosen such that $\alpha\rho < \mu_0$ where $\mu_0 \simeq 2.4$ is the first zero of $J_0(r)$. The scalar product on the boundary ∂D_- is $(\varphi,\psi)_{\partial D_-} = \int_{\partial D_-} \rho\, \varphi\bar{\psi}\, d\theta$. Note that if α increases ($M \to 1$) the admissible radius $\rho \to 0$, which leads to reduce the step of the mesh.

3.2.2. *Right disk D_+*

Around the trailing edge we now define the radius $r = \sqrt{(x-L)^2 + (y-\eta)^2}$. In the right disk the spectral representation depends on which system, Eq. 6 or Eq. 7, is solved:

- If φ_{D_+} is solution of Eq. 6, then the expansion (8) is valid in $D_+\backslash\Gamma_+$ for the field φ_{D_+} by replacing D_- with D_+.
- If φ_{D_+} is solution of Eq. 7, as it does not obey to a homogenous Neumann condition on the plate, the representation 8 is no longer valid. To overcome this difficulty we introduce the function φ_S^- defined in the disk D_+ as $\varphi_S^- = \zeta^-(y)e^{i\alpha x/M}$. Then the field $\psi = \varphi_{D_+} + \varphi_S^-$ satisfies a homogenous Neumann condition on the plate and the expansion 8 is valid in $D_+\backslash\Gamma_+$ for ψ.

In the previous article [3], the problem 7 was not solved. Another one involving the unknown function $\varphi_c + \varphi_S^-$ where the function φ_S^- was extended to the half space $x > d$) has been used. Thus we had $\varphi_S^- \approx e^{kH/M}e^{i\alpha x/M}$ on the upper part of the duct, and therefore when $M \to 0$, the exponential term became very large which led to refine the mesh a lot in order to avoid instabilities. In practice the numerical method was efficient only for Mach numbers above $M = 0.3$. In our new approach the unknown function $\varphi_c + \varphi_S^-$ is only considered in the disk D_+ and its maximum value is only of order $e^{k\rho/M}$ which is kept small when $M \to 0$ by reducing ρ.

As in the case of the exterior domains, boundary conditions on the disks can be deduced for the solution in the disks. They involve the following Dirichlet-to-Neumann operators defined as:

$$T_{D_\pm}\phi = \sum_{n=0}^{\infty} \alpha \frac{J'_{\frac{n}{2}}(\alpha\rho)}{J_{\frac{n}{2}}(\alpha\rho)} (\phi, b_n)_{\partial D_\pm} b_n(\theta).$$

3.2.3. *Singularity coefficients*

The Kutta-Joukowski condition imposes the velocity to be bounded close to the trailing edge of the plate. Using the asymptotic behavior of the Bessel function $J_{1/2}$: $J_{1/2}(\alpha r) \approx \sqrt{2\alpha r/\pi}$ when $r \to 0$, combined with the spectral representations of the diffracted field ψ in the disk D_+, the asymptotic behavior of ψ in D_+ is $\psi \approx \sigma(\psi)\sqrt{r}b_1(\theta)$ when $r \to 0$. The singularity coefficient is given by

$$\sigma(\psi) = \sqrt{\frac{2\alpha}{\pi}} \frac{(\psi, b_1)_{\partial D_+}}{J_{\frac{1}{2}}(\alpha\rho)}.$$

This is the only singular behavior ($\mathbf{v} = \nabla\varphi \approx 1/\sqrt{r}$), since the other Bessel functions $J_{n/2}$, $n > 1$ have an asymptotic behavior in $r = 0$ varying like $r^{n/2}$. Moreover since $\nabla\varphi_S^-$ is regular near the trailing edge, σ is also the singularity coefficient of φ_{D_+}.

Thanks to such spectral representations, the diffraction problems Eq. 6 and Eq. 7 can be set in a bounded domain, which then leads to a problem adapted to a numerical resolution.

3.3. *Reduction to a bounded domain*

The fields φ and φ_c are sought in the bounded domain $\Omega_R \backslash D_\pm$, where finite elements can be introduced. The incident wave is chosen as a propagative mode of the duct $\varphi_{inc} = e^{i\beta_m x}\,\theta_m(y)$, and then the total acoustic field φ satisfies the system:

$$\begin{cases} (\Delta + \alpha^2)\varphi = 0 & \text{in } \Omega_R \backslash D_\pm, \\ \partial\varphi/\partial y = 0 & \text{on } \partial D \cup \Gamma_m^- \cup \Gamma_m^+, \\ \partial\varphi/\partial n = -T_{\Sigma_\pm}\varphi + f_\pm & \text{on } \Sigma_\pm, \\ \partial\varphi/\partial n = -T_{D_\pm}\varphi & \text{on } \partial D_\pm, \end{cases} \tag{9}$$

where $f_+ = 0$ and $f_- = -2i\beta_m\varphi_{inc}$, whereas the correction field φ_c satisfies:

$$\begin{cases} (\Delta + \alpha^2)\varphi_c = 0 & \text{in } \Omega_R \backslash D_\pm, \\ \partial\varphi_c/\partial y = 0 & \text{on } \partial D \cup \Gamma_m^-, \\ \partial\varphi_c/\partial y = -\partial\tilde{\varphi}_S/\partial y & \text{on } \Gamma_m^+, \\ \partial\varphi_c/\partial n = -T_{\Sigma_\pm}\varphi_c & \text{on } \Sigma_\pm, \\ \partial\varphi_c/\partial n = -T_{D_\pm}\varphi_c + g_\pm & \text{on } \partial D_\pm, \\ [\varphi_c]_{\gamma_\pm} = -\tilde{\varphi}_S|_{\gamma_\pm}, & \text{and} \quad [\partial\varphi_c/\partial x]_{\gamma_\pm} = -i\,\alpha\tilde{\varphi}_S/M|_{\gamma_\pm}\,, \end{cases} \tag{10}$$

with $g_- = 0$ and $g_+ = -T_{D_+}\varphi_S^- - \partial\varphi_S^-/\partial n$. Once φ and φ_c are determined, the Kutta-Joukovski condition leads to choose the vortex sheet coefficient F such that $\sigma(\varphi) + F\sigma(\varphi_c) = 0$.

4. Numerical results

The domain of calculation is meshed non-uniformly with triangular elements (note that each circle is approached with a polygon, but the resulting error is under control in the sense

that it is of the same order that the P1 finite elements error). The bounded domain, in which the fluid streams as a uniform flow, is then transformed using the dilatation presented in section 2, in order to obtain an equivalent medium at rest. The mesh is chosen such that it contains at least ten points per the shortest wavelength to ensure a good discretization of oscillating phenomena (5000 to 20000 degrees of freedom). This condition has been checked everywhere in the mesh, and in particular behind the plate where the grid needs to be refined to take into account the short vortex sheet wavelength. We use standard Lagrange finite elements approximation ($P1$ or $P2$, depending on the desired accuracy). The numerical resolution is achieved using the code *Melina* [20], which is an open source set of subroutines written in *Fortran*. Note that to find the solution, it is not necessary to discretize the inside of the disks. But in order to have a full graphic representation we computed the solution inside the disks using the spectral representations.

4.1. *Diffraction results*

All the results presented below have been obtained using eigth terms in the modal representations outside the bounded domain (always greater than the number of propagative modes, typically from two to four modes) and thirty terms in the spectral representations inside the disks. Also all the results are presented in the "physical" domain. As first results, we present two examples of the velocity potential diffracted by a plate. The plate length is greater than the wavelength of the wake in Fig. 5, whereas it is lower in Fig. 6. Iso-contours of the real part of the total velocity potential $\varphi_t = \varphi + F\varphi_S$ are plotted on both figures. In our simulations, the waveguide height is $H = 4$ and the plate is placed at $\eta = 3H/4$. The acoustical incident wave corresponds to the first antisymmetric transversal mode of the waveguide ($n = 1$). In this configuration, the normal derivative of the incident velocity potential is not equal to zero on the plate, which ensures that a diffracted field is excited (symmetric modes as the mode $n = 0$ are not diffracted for centered plates). In both figures, the fluid flows from left to right and the Mach number is $M = 0.3$.

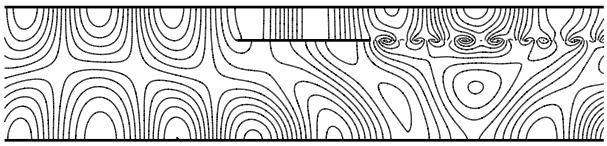

Fig. 5. Real part of the total velocity potential for a Mach number $M = 0.3$ and with a plate length $L = 4$ (15 isolines from -0.7 to 0.7). The incident wave, of acoustic wavenumber $k = 2$, corresponds to the first antisymmetric guided mode.

In Fig. 5, the incident acoustic wavenumber is $k = 2$ and the plate length is $L = 4$. The three first modes ($n = 0, 1, 2$) of the waveguide are propagative. The wavelength of the wake is $\lambda_S = 2\pi M/k \sim 0.94$, and the antisymmetric propagative guided mode wavelengths are $\lambda_1^+ \sim 4.56$ and $\lambda_1^- \sim -2.33$. Considering the vorticity wavelength as a characteristic length, the plate can be considered here as a long one. Therefore the region between the plate and

the upper wall of the waveguide can be approximated with a waveguide of height $H' = 1.0$, in which only the plane wave $n = 0$ can propagate. Fig. 5 indicates that this approximation seems to be correct: indeed the incident wave is transformed into a plane wave above the plate, whereas an almost first antisymmetric mode is selected below the plate. The wake can be clearly seen downstream the plate. It is possible to distinguish the presence of a reflected wave travelling upstream (the $n = 1$ mode is distorded).

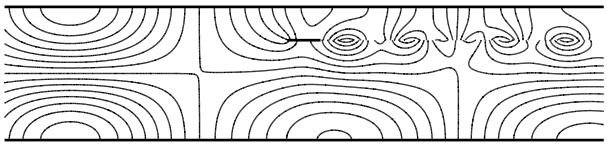

Fig. 6. Real part of the total velocity potential for a Mach number $M = 0.3$, $k = 1$ and with a plate length $L = 1$ (15 isolines from -0.9 to 0.9).

In Fig. 6, the incident acoustic wavenumber is $k = 1$ and the plate length is $L = 1$. Here, only the two first modes ($n = 0, 1$) of the waveguide are propagative, and the antisymmetric guided modes wavelengths are $\lambda_1^+ \sim 15.78$ and $\lambda_1^- \sim -5.94$. In that case, the plate is shorter than the characteristic length of the vortex sheet ($L < \lambda_S \sim 1.88$). The plane wave $n = 0$ is the only mode able to propagate in the region above the plate. But a plane wave is not observed above the plate because the evanescent modes do not vanish spatially in presence of a so short plate. Note that the field diffracted upstream is very weak. The wake looks "stronger" on Fig. 6 than on Fig. 5 (larger rolls): this is due to the fact that the characteristic transversal extent of the wake and its wavelength are proportional to the ratio M/k.

4.2. *Wake amplitude*

4.2.1. *Mach number dependance*

Determinations of the diffracted field, as presented before, have been made for several plate lengths, frequencies k and Mach numbers in order to characterize the variations of the wake amplitude F versus the Mach number. A semi-analytical solution for the field diffracted by a semi-infinite plate has been derived from calculations involving the Wiener-Hopf method [5]. For small Mach numbers and a fixed frequency, the amplitude of the wake is theoretically found proportional to the square root of the Mach number: $|F| = \alpha\sqrt{M}$. One can expect that the qualitative behavior of the field diffracted by a sufficiently long plate will be close to the one induced by a semi-infinite plate. Therefore the ability of our code to extract the amplitude of the vortical field gives us two opportunities: first for large plate lengths, comparison between numerical results and analytical results can give a validation to our code. Also, by extracting numerically the dependence of the wake amplitude $|F|$ as a function of the Mach number M, we are able to check the validity of the law $|F| = \alpha\sqrt{M}$ for small plate lengths. Indeed we suspect that it remains valid because Kutta-Joukowski

is a local condition which does not involve the plate length.

Numerical results are plotted in logarithm scale in Fig. 7, for different plate lengths ($L = 1$ and $L = 4$) and for different frequencies of incident waves ($k = 1$ and $k = 2$). It first appears that for intermediate values of the Mach number ($0.02 < M < 0.5$ for $k = 1$ and $0.04 < M < 0.3$ for $k = 2$), the vortex sheet amplitude obeys the law $\log |F| = a \log M + b$ with $a = 1/2$ and thus $|F| = \alpha\sqrt{M}$ as in the semi-infinite plate case. More precisely we have calculated the parameters α and β such that $|F| = \alpha\sqrt{M} + \beta$ for various values of L and k. In all cases we have found that $\beta \approx 0$. For instance in the case $L = 8$, we get $\alpha = 1.0007$ and $\beta = 0.017$ for $k = 1$ and $\alpha = 1.4756$ and $\beta = 0.0028$ for $k = 2$.

For low Mach numbers ($M < 0.04$) and for large Mach numbers ($M > 0.3$), we observe that the law $|F| = \alpha\sqrt{M}$ is no longer valid. For low Mach numbers this is related to the mesh grid step, which is not well suited when the wavelength and the spatial extent of the vortex sheet, both proportional to the ratio M/k, are too small. For the thinest mesh we have used, we get that results are valid for $M/k > 0.02$ (a thiner mesh would lead to the same result but with a smaller lower bound). This is the reason why when k is lower, the curve $F(M)$ can be calculated for lower Mach numbers. However for large mach numbers the change of behavior of the curve $F(M)$ is related to the presence of singular frequencies. For a fixed value of the Mach number, the diffraction problem has been proven to be well-posed, except for isolated values of the frequency $k(M)$ [3]. In a same way for a fixed frequency isolated critical Mach numbers exist. For these critical values, the diffracted field is not unique, and numerically, the computation of the diffracted potential velocity leads to inverse a non-inversible matrix. We have shown that the "peaks" on the curve $F(M)$ corresponds to these critical values.

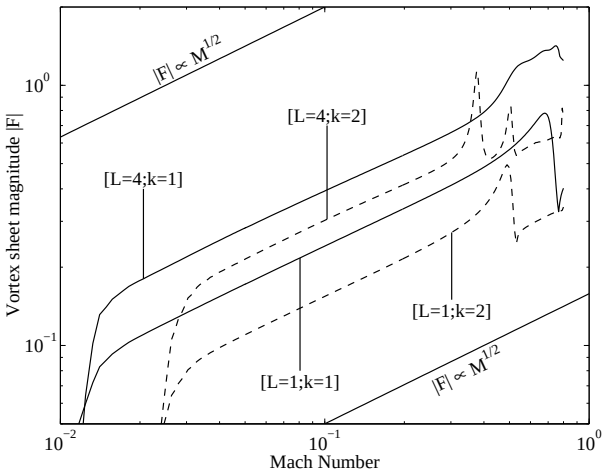

Fig. 7. Logarithm of the vortex sheet magnitude at the trailing edge as a function of the logarithm of the Mach number. Results are presented for two different lengths of the plate ($L = 1$ and $L = 4$), and for two different values of the acoustic wavenumber ($k = 1$ and $k = 2$). The curves $|F| \propto M^{1/2}$ indicate the slope corresponding to a square root law.

4.2.2. *Plate length dependance*

The dependance of the wake amplitude versus the plate length has also been characterized. In the appropriate ranges of Mach numbers for which we have $|F| = \alpha\sqrt{M}$ where α is not M dependant (see Fig. 7), the parameter $\alpha(L) = \partial|F|/\partial\sqrt{M}$ is presented in Fig. 8, for two frequencies ($k = 1$ and $k = 2$) as a function of the plate length. By simple calculus it can be proven that for a fixed value of the Mach number the diffracted amplitude $|F| = |\sigma(\varphi)| \,/\, |\sigma(\varphi_S)|$ is bounded by $\sqrt{L}$. Briefly it follows from the fact that $|\sigma(\varphi_S)|$ (created by the vortex sheet) is independant of L whereas the diffracted acoustic field φ_a (created by a source located on the plate) depends on L. More precisely it is proven that $|\sigma(\varphi)| = |\sigma(\varphi_a)|$ is bounded by the square root of the plate length. In fact as Fig. 8 shows it, α is varying like $\sqrt{L}$ for the small lengths of the plate.

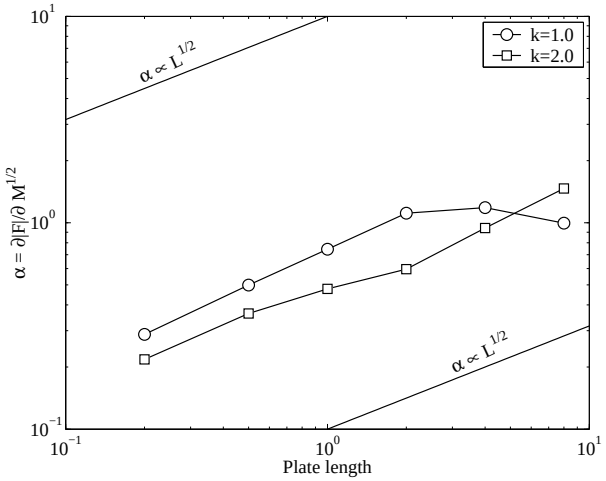

Fig. 8. Parameter $\alpha = \partial|F|/\partial\sqrt{M}$ versus the plate length, for the frequencies $k = 1$ and $k = 2$.

4.3. *The dissipated sound power*

To characterize the acoustic properties of the combination of the plate and of the vortex sheet, the acoustic energy dissipated during the production of vorticity at the edge of the plate can be evaluated. Such evaluation has been carried out and compared to experiment in the case of an infinite plate [6].

Let us recall that the total velocity potential $\varphi_t = \varphi + F(\varphi_c + \tilde{\varphi}_S)$ satisfies the problem:

$$\begin{cases} (\Delta + \alpha^2)\varphi_t = 0 & \text{in } \Omega_R/S, \\ \partial\varphi_t/\partial y = 0 & \text{on } \partial D \cup \Gamma, \\ [\varphi_t]_S = F\, e^{i\alpha x/M} & \text{and} \qquad [\partial\varphi_t/\partial y]_S = 0, \end{cases}$$

where the bounded domain Ω_R surrounding the plate and delimited by the two boundaries

$\Sigma_\pm$ has been defined in section 3. Introducing the acoustic flux through any surface Σ:

$$\Pi_\Sigma(\varphi) = \int_\Sigma \Im m\left(\frac{\partial\varphi}{\partial x}\bar{\varphi}\right)\, dy,$$

and integrating the Helmholtz equation over the domain Ω_R leads to the energy balance:

$$\Pi_{\Sigma_+}(\varphi_t) - \Pi_{\Sigma_-}(\varphi_t) - \int_{S_R} \Im m\left(\frac{\partial\varphi_t}{\partial y}\left[\bar{\varphi}_t\right]_{S_R}\right)\, dx = 0.$$

S_R is the piece of the wake included in Ω_R. Following Howe [6], we define the dissipated energy as:

$$\Pi_D = \Pi_{\Sigma_+}(\check{\varphi}) - \Pi_{\Sigma_-}(\check{\varphi}),$$

where $\check{\varphi} = \varphi + F\varphi_c$ represents the acoustic part of the total velocity potential, $\tilde{\varphi}_S$ standing for the hydrodynamic part.

Remark 1: If $\check{\varphi} = \varphi$ (case $F = 0$ corresponding to the diffraction problem without vortex sheet), the dissipated energy Π_D vanishes. This justifies why Π_D evaluated for $\check{\varphi}$ with $F \neq 0$ characterizes the energy dissipated by the vortex sheet.

Using the property that the acoustic field $\check{\varphi}$ can be decomposed on the duct modes (which is not the case for the hydrodynamic field $\tilde{\varphi}_S$), the dissipated energy takes the form:

$$\Pi_D = 2\beta_m \Re e\left[(\overline{\varphi_{inc}}, \theta_m)_{\Sigma_-}(\check{\varphi}, \theta_m)_{\Sigma_-}\right] - \sum_{n\leq\alpha H/\pi} \beta_n \left[\left|(\check{\varphi}, \theta_n)_{\Sigma_+}\right|^2 + \left|(\check{\varphi}, \theta_n)_{\Sigma_-}\right|^2\right],$$

where $\theta_n(y)$ and φ_{inc} are defined in sections 3.1 and 3.3. Note that the sum is limited to the propagative modes of the duct, the evanescent modes carrying no energy away of the plate. This expression is useful since the coefficients $(\check{\varphi}, \theta_n)_{\Sigma_\pm}$ are computed to take into account the Dirichlet-to-Neumann operators $T_{\Sigma_\pm}$.

Remark 2: We have prefered to measure the energy dissipation in the "Helmholtz space" (associated to a fluid at rest). It is easy to deduce the energy balance in the "physical space" (in presence of a fluid in motion) by using the Prandtl-Glauert transformation: $\hat{\varphi}(\hat{x}, \hat{y}) = \varphi(x, y)e^{i\alpha M\hat{x}}$ where $\hat{x} = x/\sqrt{1-M^2}$. Then the flux through a surface Σ in the Helmholtz space:

$$\Pi_\Sigma(\hat{\varphi}) = \int_\Sigma \Im m\left(\frac{\partial\hat{\varphi}}{\partial\hat{x}}\bar{\hat{\varphi}}\right)\, dy,$$

becomes

$$\Pi^M_\Sigma(\varphi) = \Pi_\Sigma(\hat{\varphi}) = \frac{1}{\sqrt{1-M^2}}\int_\Sigma \left[(1-M^2)\Im m\left(\frac{\partial\varphi}{\partial x}\bar{\varphi}\right) + kM\left|\varphi\right|^2\right]\, dy,$$

in the physical space, which is the usual expression [6].

On Fig. 9 is represented the dissipated power Π_D/Π_0 versus the Mach number for a plate of length $L = 1$ and the frequencies $k = 1$ and $k = 2$. $\Pi_0 = \beta_m\left|(\varphi_{inc}, \theta_m)_{\Sigma_-}\right|^2$ is the incident acoustic power. In both cases, the dissipated power varies linearly versus the Mach

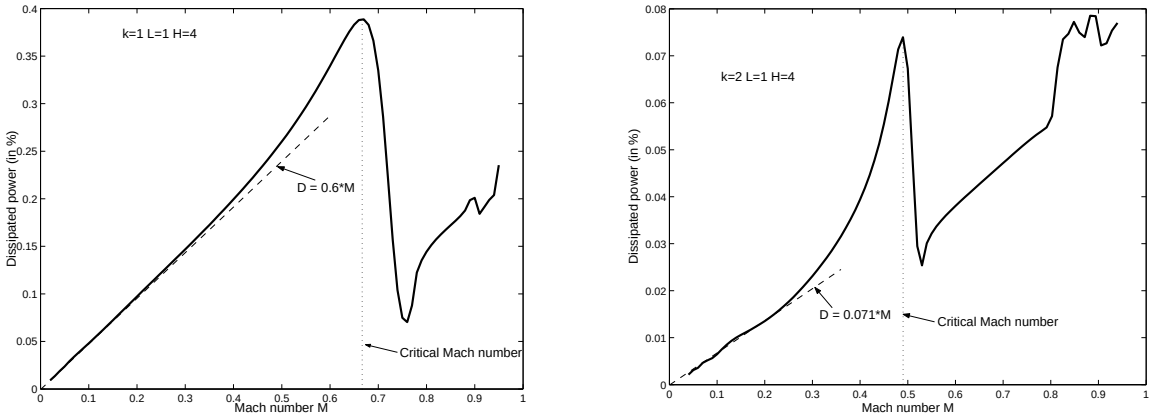

(a) $k = 1$, $L = 1$ (b) $k = 2$, $L = 1$

Fig. 9. Π_D/Π_0 versus M

number for small values of M, as in the case of a semi-infinite plate [6]. For Mach numbers larger than 0.85 curves are not significant because numerical instabilities occur (mesh not enough refined in view of high wavenumbers in Helmholtz space). The dependance of the

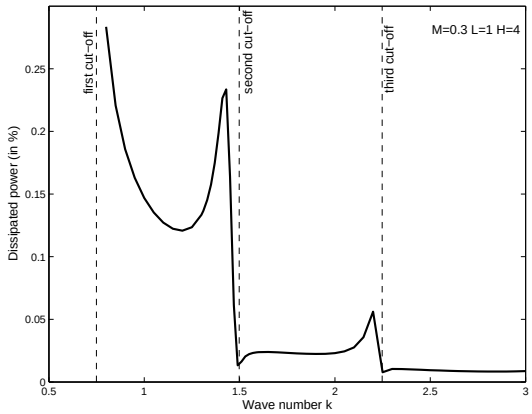

Fig. 10. Π_D/Π_0 versus k for $M = 0.3$ and $L = 1$.

dissipated power versus the frequency is depicted on Fig. 10 in the particular case $M = 0.3$. The cut-off frequencies of the duct are defined as $k_c^{(n)} = n\pi\sqrt{1 - M^2}/H$, $n \geq 1$. Note that the dissipated power simply vanishes for $k < k_c^{(1)} = 0.75$ (not represented on Fig. 10): in this case only the first mode of the duct (the plane one) can propagate, which can not interact with the plate ($\partial\varphi_{inc}/\partial y = 0$ on the plate). As in [6] (where the configuration is slightly different: incident wave only above the plate, chosen to be equal to zero below the plate) we found that the dissipated power reaches non-negligible values only below $k_c^{(2)} = 1.50$, and

different and we observe regimes separated by the cut-off frequencies.

5. Extension of the method

The presented method may be easily extended to more complicated situations: for example, the case of two parallel plates or aligned plates. For parallel plates, the vortex sheets induced by the trailing edges interact with each other when we apply the Kutta-Joukowski conditions on the trailing edges. The case of aligned plates is more interesting. Here, in addition to the coupling between the vortex sheets, there is an interaction of the wake induced by the upstream plate with the second plate. This interaction raises complicated questions concerning the choice of the correct boundary conditions on the second plate. If a rigid plate condition is used, this implies that the vorticity carried by the wake cancels when reaching the leading edge of the downstream plate. The physical mechanism responsible of this cancellation is not obvious.

Such problem appeared when Howe studied the case of two semi-infinite plates aligned and separated by free space (perforated screen or organ pipe [21]). Two different boundary conditions on the downstream plate were considered. First, a rigid boundary condition $\partial\varphi/\partial y = 0$ was considered [16]. Later Howe [17] claimed that it was wrong to neglect the vorticity on the plate. Considering a viscous model Howe took into account the two boundary layers present on the plate surfaces, which can support Tollmien-Schlichting waves. The interaction of the vortex-sheet with the leading edge leads to the creation of vorticity in the boundary layers. This vorticity is convected in the layers and produces displacement thickness fluctuations which are antisymmetric about the plate, of wave number κ and of amplitude v_0 (modelized with the boundary condition $\partial\varphi/\partial y = v_0 e^{i\kappa x}$). The quantity v_0 is determined by applying a Kutta-Joukowski condition at the leading edge of the downstream plate (called the unsteady Kutta-Joukowski condition [22]), and a study of the boundary layer disturbances gives $\kappa = 5k/3M$ (compared with k/M, the wavelength of the vortex sheets) [17]. For more details, the evolution of these Tollmien-Schlichting waves near a plate leading edge in the presence of viscosity have been carefully characterized in [23] using matched asymptotic expansions.

We denote by Γ_1 and Γ_2 the two plates and S_1 and S_2 the vortex sheets (see Fig. 11). The diffracted field satisfies the same equations as in the one plate case, but with the

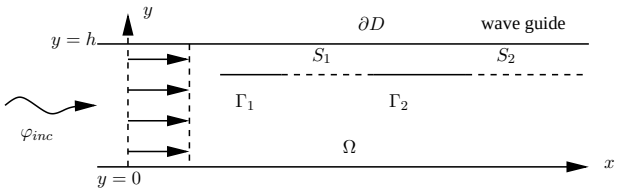

Fig. 11. Geometry of the two plates problem.

additional vortex sheet conditions $[\varphi_d]_{S_i} = F_i e^{i\alpha x/M}$ and $[\partial\varphi_d/\partial y]_{S_i} = 0$ for $i = 1$ or 2, and

the boundary layer condition $\partial\varphi_d/\partial y = F_3 e^{i\tilde{\kappa}x}$ on Γ_2. The quantity $\tilde{\kappa} = (\alpha/M)(5-2M^2)/3$ is the boundary layer wavenumber after the transformation "uniform flow-fluid at rest". The vortex sheets are eliminated by introducing the vortex sheet functions φ_{S_1} and φ_{S_2} satisfying: $[\varphi_{S_i}]_{S_i} = e^{i\alpha x/M}$ and $[\partial\varphi_{S_i}/\partial y]_{S_i} = 0$, for $i = 1$ or 2. Then the diffracted field is sought in the form $\varphi_d = \varphi_a + F_1\varphi_{S_1} + F_2\varphi_{S_2} + F_3\varphi_3$ where φ_a is the solution without the vortex sheet and φ_3 is the field generated by the boundary layers. Using the Kutta-Joukowski conditions at the two trailing edges and at the leading edge of Γ_2, a linear system of three equations is obtained for the unknowns F_1, F_2, and F_3.

The calculation domain, including four disks, is shown in Fig. 12. The real part of the

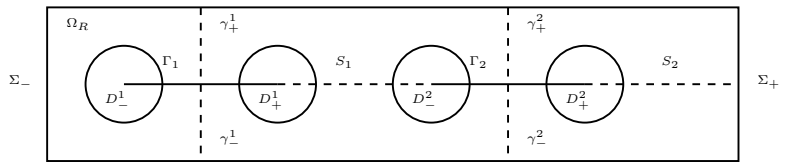

Fig. 12. Numerical domains of the two plates problem

total velocity potential is shown for two plates each of length $L = 4$, at the frequency $k = 1$ and the Mach number $M = 0.3$ in Fig. 13 (for a rigid boundary condition on the second plate) and in Fig. 14 (for a boundary layer condition). In the first case, the wakes have

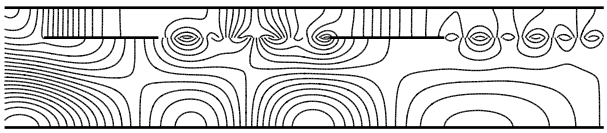

Fig. 13. Real part of the total velocity potential for two plates $L = 4$, $k = 1$ and $M = 0,3$. 21 isolines between -1 and 1. $F_1 = 0.49 + 0.05i$ and $F_2 = 0.24 - 0.48i$. $|F_1| = 0.49$ and $|F_2| = 0.54$.

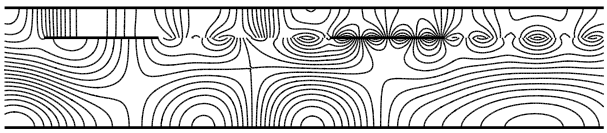

Fig. 14. Total velocity potential for $L = 4$, $k = 1$ and $M = 0,3$. Re et Im: 21 isolines between -1.5 and 1.5. $F_1 = -0.47 + 0.43i$, $F_3 = 0.74 + 2.68i$ and $F_2 = 0.25 - 0.71i$. $|F_1| = 0.64$, $|F_3| = 2.78$ and $|F_2| = 0.75$

nearly the same amplitude whereas in the second case the amplitude F_3 is four times larger than F_1 and F_2.

The natural question to ask is which boundary condition on the downstream plate is the better one? It seems clear that the boundary layer condition has a better chance of

being valid in the case of a long downstream plate (Howe [17] considered an infinite plate). Indeed the growth rates of the Tollmien-Schlichting waves is small when the boundary layer is thin. In the case of a long plate ($L \gg \lambda_\kappa$ where λ_κ is the wavelength associated to the wavenumber κ), the boundary layer can grow enough to become unstable. But in our case of a short plate, this layer may remain stable. In the case of a configuration similar to ours, a theoretical study [1] was not able to reject either one of the two boundary conditions. Their configuration consisted of an infinite plate lying along the centerline of a duct and having a single transverse slot. In that configuration the slot width does not exceed the width of the duct, and these two lengths are small compared to the characteristic acoustic wavelength. In contrast our configuration is one in which the slot width, the duct height, and the acoustic wavelength are of the same order. In additions the vortex sheet displacement is represented using degenerate Kelvin-Helmholtz instability waves [1] (one of them growing linearly with the distance downstream). In spite of these differences, it is helpful to mention the results of the study in [1]. There, a solution was first obtained which did not take into account the vorticity ejection from the slot. Then the displacement-thickness waves on the downstream boundary layers were included in the theoretical model. Although this study did not allow one to reject either one of the boundary conditions, it showed that the linearized theory breaks down near the trailing edge (large amplitude of the displacement of the vortex sheet) when the influence of ejected vorticity at the trailing edge of the slot is neglected. Moreover, the linearized theory led to much larger predictions of the amount of acoustic energy produced at the slot.

This modelization question is also present when the flow is non-uniform (unstable shear layer, for example). In this case it is no longer a wake that interacts with the plate but a Kelvin-Helmholtz instability. Then Tollmien-Schlichting instabilities have a greater chance to be generated. However, the choice of the boundary conditions to impose on the plate is still an open question in this case. Different boundary conditions have been suggested: $p = 0$ [24] or $\partial\varphi/\partial y = v_0^{\pm} e^{i\kappa^{\pm} x}$ (the presence of Tollmien-Schlichting waves of differents wavenumbers $\kappa^{\pm}$ on the two sides of the plates) [21]. Another approach consists in taking into account the instability inherent of the incident flow. Then the Tollmien-Schlichting instability is ignored and the Kutta-Joukowski condition is applied [25]. But the author showed that the solution satisfying the Kutta-Joukowski condition is not necessarily the correct one.

6. Conclusion

The acoustic diffraction of a wave by a finite plate in a uniform flow has been studied numerically with a finite elements method in the frequency domain. A wake, modeling the interaction between the acoustic waves and the incident flow has been introduced behind the plate. A numerical scheme, whose convergence we proved, was used to study a large range of subsonic Mach numbers. We proved that for a fixed frequency, the amplitude of the wake varies like $|F| = \alpha\sqrt{LM}$ for a small Mach number and a short plate length. Therefore, the already known result in the case of a semi-infinite plate (where the amplitude of the wake

varies like the square root of M) remains true in the case of a finite plate. In addition, the dissipated power was proven to vary linearly with M for small values of the Mach number, again same as in the semi-infinite plate case. The advantage of our method is that it allows the extension to more complicated geometries, like several aligned plates. The case of two plates was considered, and because the modelization of the boundary conditions on the downstream plate is still an open question, we tried two models. As reference solutions, our numerical results could be used to help to explain experimental observations.

The next step would be to take into account the presence of a shear flow. This case brings complicated theoretical and numerical problems. First, it is not possible to derive from the Euler's equations an elliptic scalar model and thus the finite elements approach is no longer easily applicable. Second, although it is possible to calculate the modes of the duct [26], so far we have been unable to get good radiation conditions. Therefore, we are currently working on another model, the Galbrun's equations [27], which is a displacement formulation. This model has two advantages: it is an elliptic equation and it is a model for which the interface condition (continuity of the normal displacement) is natural. However, this approach raises new difficulties [28] whcih we are in the pocess of resolving.

Acknowledgment

This work has benefited the support of the European Community through a fellowship provided to one of the author (S.J.), in the frame of the project SILENCE(R) (for "Significantly Lower Community Exposure to Aircraft Noise", Contract N° G4RD-CT-2001-00500, Project N° GRD1-2000-25297).

References

1. M. C. Quinn and M. S. Howe, Absorption of sound at a slot in a splitter plate in a mean-flow duct, *J. Fluid Mech.*, **168** (1986) 1.
2. M. S. Vasudevan, P. A. Nelson and M. S. Howe, An experimental study of the influence of mean flow on acoustic dissipation by vorticity production at edges, *IUTAM Symp. Aero- and Hydro-acoustics. Lyon. 3-5 July 1985*, (1985).
3. A.-S. Bonnet-Ben Dhia, L. Dahi, E. Lunéville and V. Pagneux, Acoustic diffraction by a plate in a uniform flow, *Math. Models Methods Appl. Sci.*, **12** (2002) 625.
4. D. S. Jones, Aerodynamic sound due to a source near a half plane, *institute of Mathematics and its Applications*, **9** (1972) 114.
5. A. D. Rawlins, Acoustic by an absorbing semi-infinite half-plane in a moving fluid, *Proc. R. S. E. (75 A)*, **7** (1976) 82.
6. M. S. Howe, Attenuation of sound due to vortex shedding from a splitter plate in a mean flow duct, *Journal of Sound and Vibration*, **105** (3) (1985) 385.
7. Mahmood-Ul-Hassan and A. D. Rawlins, Two problems of waveguides carrying mean fluid flow, *Journal of Sound and Vibration*, **216** (1998) 712.
8. O. Pironneau, *Méthode des éléments finis pour les fluides*, (Masson, 1988), pp. 41-44.
9. K. Stewartson, On the flow near the trailing edge of a flat plate, II., *Mathematika*, **16** (1969) 106.

10. A. F. Messiter, Boundary-layer flow near the trailing edge of a flat plate, *SIAM J. Appl. Math.*, **18** (19) 241.
11. L. Pong-Jeu, P. Dartzi and Y. Dun-Yann, Numerical Simulation of Trailing-Edge Acoustic/Vortical Interaction, *AIAA Journal*, **33** (1995) 785.
12. C. Bogey, C. Bailly and D. Juvé, Computation of the sound radiated by a 3-D jet using Large Eddy Simulation, *AIAA* (2000) 2000.
13. T. Colonius, S. K. Lele and P. Moin, Sound generation in a mixing layer, *J. Fluid Mech.*, **330** (1997) 375.
14. G. Raugel, PhD. thesis, Université de Rennes (1978).
15. B. Noble, *Methods based on Wiener-Hopf Technique* (Pergamon Press, New York, 1958).
16. M. S. Howe, The influence of vortex shedding on the diffraction of sound by a perforated screen, *J. Fluid Mech.*, **97** (1980) 641.
17. M. S. Howe, The role of displacement thickness fluctuations in hydroacoustics, and the jet-drive mechanism of the flue organ pipe, *Proc. R. Soc. Lond. A*, **374** (1981) 543.
18. V. Pagneux, Propagation acoustique dans les guides à section variable et effets d'écoulement, PhD. thesis, Université du Maine (1996).
19. M. Lenoir and A. Tounsi, The localized finite element method and its appication to the two-dimensional sea-keeping problem, *SIAM J. Numer. Anal.*, **25** (1988).
20. D. Martin, *On line documentation of the code* MÉLINA *http://perso.univ-rennes1.fr/daniel.martin/melina/www/homepage.html*
21. M. S. Howe, On the theory of unsteady shearing flow over a slot, *Phil. Trans. R. Soc. Lond. A*, **303** (1981) 151.
22. D. G. Crighton, The Kutta condition in unsteady flow, *Ann. Rev. Fluid. Mech.*, **17** (1985) 411.
23. M. E. Goldstein, The evolution of Tollmien-Schlichting waves near a leading edge, *J. Fluid Mech.*, **127** (1983) 59.
24. D. S. Jones, A linear model of a finite amplitude Helmholtz instability, *Proc. R. Soc. Lond. A*, **338** (1974) 17.
25. M. E. Goldstein, The coupling between flow instabilities and incident disturbances at a leading edge, *J. Fluid Mech.*, **104** (1981) 217.
26. B. Nilsson, Scattering of stable and unstable waves in a flow duct, *Q.J. appl. Math.*, **51** (1998) 599.
27. H. Galbrun, *Propagation d'une onde sonore dans l'atmosphère terrestre et théorie des zones de silence*, (Gauthier-Villars, Paris, 1931).
28. E. Bécache, A.-S. Bonnet-Ben Dhia and G. Legendre, Perfectly matched layers for the convected Helmholtz equation, *SIAM J. Numer. Anal.*, **42** (1) (2004) 409.